Bainite Formation in Carbon and Nitrogen enriched Low Alloyed Steels: Kinetics and Microstructures

J. Teixeira, S. Catteau, Hugo P. van Landeghem, J. Dulcy, M. Dehmas, A. Redjaimia, S. Denis, M. Courteaux

Bainite formation in carbon and nitrogen enriched low alloyed steels: kinetics and microstructures

Julien Teixeira[1,2], Simon D. Catteau[1,2,3], Hugo P. Van Landeghem[1,2], Jacky Dulcy[1], Moukrane Dehmas[1,2], Abdelkrim Redjaïmia[1,2], Sabine Denis[1,2], Marc Courteaux[3]

[1]*Université de Lorraine, CNRS, IJL, F-54000 Nancy, France*

[2]*Labex DAMAS "Design of Alloy Metals for Low-mass Structures", Université de Lorraine, France*

[3]*PSA Peugeot-Citroën, Centre Technique de Belchamp, F-25420 Voujeaucourt, France*

Abstract

The effect on the bainite formation of carburizing (0.6wt%C), nitriding (0.12wt%C-0.25wt%N) and carbonitriding (0.7wt%C-0.25wt%N) of a 23MnCrMo5 low-alloyed steel in the austenitic field was examined by in situ high-energy synchrotron X-ray diffraction (HEXRD) and transmission electron microscopy. The enrichment in nitrogen induces strong acceleration of the bainite transformation kinetics in carbonitrided steel compared to carburized steel, despite the γ-stabilizing character of nitrogen. This is attributed to the nucleation of ferrite on CrN nitrides, which precipitated during the enrichment, either at γ grain boundaries or intragranularly. AlN, VN and $MnSiN_2$ nitrides were observed as well, with much smaller number density. They formed frequently aggregates with the CrN nitrides. The bainite microstructure is much finer than in initial or carburized steel. It shares some common features with intragranularly nucleated bainite, i.e. acicular ferrite. From HEXRD, the chronology of the phase formation (ferrite and precipitates) during bainite formation as well as cell parameter evolutions are analyzed.

Keywords

Carbonitriding, Phase transformation kinetics, Bainite microstructure, Low-alloyed steel, TEM, High energy synchrotron X-ray diffraction

1 Introduction

The influence of carbon content on austenite decomposition in steels was largely described in literature (e.g. [Constant, Henry, Charbonnier, 1992]). Conversely, nitrogen effects on the austenite decomposition were less examined. Most studies dealt with the model Fe-N system (e.g. [Jiang 2008, Nakada 2013]). In this case, product phases are ferrite and γ'-Fe_4N. Regarding the Fe-C-N system, some studies considered the tempering of martensite (e.g. Refs. [Böttger 1996, Cheng 1992]). Very few studies were conducted on multicomponent alloys. For instance, Simon et al. [Simon 1974] examined a 30CrMo4 steel enriched in carbon and nitrogen. Unexpectedly, the continuous cooling kinetics was faster for increased nitrogen amounts despite the γ-stabilizing character of nitrogen. This observation was ascribed to the formation of carbonitrides during the carbonitriding treatment.

The aim of this study is to analyse the decomposition of carbon and nitrogen enriched austenites of a low-alloyed 23MnCrMo5 steel in isothermal conditions. Enrichment treatments are done at 900°C, where phases present at equilibrium are austenite in case of enrichment with carbon, and austenite + CrN nitride in the case of enrichments with nitrogen. Concentration levels in solid solution in austenite are in the range 0.1-0.6 wt%C and 0.25 wt%N. Mass fraction of CrN nitrides is in the range 0.3-0.6 wt%. This paper focuses on the bainite formation, which is examined by using in situ high-energy synchrotron X-ray diffraction (HEXRD), scanning and

transmission electron microscopies (SEM, TEM). HEXRD was already used to study the bainite transformation but almost exclusively in silicon-alloyed steels leading to carbide-free bainite [Hell 2011, Babu 2005, Stone 2008, Chen 2009]. Except in [Dutta 2014], bainite transformation accompanied by formation of precipitates was not considered so far. In Sections 3 to 5, HEXRD is used in combination with TEM to determine the nature and amount of the precipitates, as well as the chronology in which the phases appear, as a function of the austenite composition in C and N. The influence of the CrN nitrides which precipitated during the enrichment treatment is analysed too. This is an overview of results which were presented in [Catteau 2016, Catteau 2017]. The last two sections analyse the evolutions of the cell parameters of ferrite and austenite which were obtained from HEXRD. On this basis, conclusions are drawn regarding the mechanism of the bainite transformation.

2 Experimental procedure

Base material of this study is a 23MnCrMo5 steel, (0.246C–1.21Mn–1.31Cr–0.237Si–0.184Ni wt%). The samples were 30 mm in length, either tubular (4 and 3 mm outer and inner diameter) or lamellar (thickness 0.5 mm, width 10 mm). They were enriched homogeneously in carbon in austenite phase field and/or nitrogen in austenite+CrN phase field by cracking methane and ammonia molecules respectively at the surface of the samples. Treatments were performed at 900°C, at atmospheric pressure in an in house thermobalance furnace which allows *in situ* monitoring of mass increase and *in situ* gas chromatography. Methods developed for the control of carbon and nitrogen concentration in solid solution were based on thermodynamic analyses of gas/solid reaction detailed in [Catteau 2014]. Homogeneity of carbon and nitrogen concentration was assessed by using a Jeol JXA- 8530F electron probe micro analyzer (EPMA). Table 1 summarizes carbon and nitrogen contents of investigated steels.

Sample	**Enrichment**	**wt%C ±0.04**	**wt%N ±0.07**	**wt%CrN ±0.03**	**Ms (°C)**	**Bs (°C)**
I	Initial	0.23	-	-	385	550 ±25
C	Carburized	0.57	-	-	260	500 ±25
N	Nitrided	0.12*	0.26	0.3	-	Between 400 and 500
C+N	Carbonitrided	0.65	0.25	0.6	205	

Table 1: Carbon and nitrogen contents in solid solution of investigated samples measured by EPMA after oil quenching from enrichment temperature. (*) N steel underwent decarburization.

HEXRD experiments on lamellar samples (N and C+N steels) were carried out at the European Synchrotron Radiation Facility (ESRF) in Grenoble, France, on the ID15B beamline. Heat treatments were made on an INSTRON® electro-thermal mechanical set-up (ETMT) installed on the beamline. The lamellar samples were heated by an electrical current, under an argon atmosphere. The X-ray beam (wavelength 0.142133 Å) crossed the sample along its width (4 mm). Rietveld analysis was performed to identify the phases, the mass fractions and lattice parameters, by using the Fullprof software. More details about experimental set-up and diffraction patterns are presented in [Catteau 2016]. HEXRD experiments on tubular samples (I and C steels) were done at the Deutsches Elektronen-Synchrotron (DESY) on the P07 beamline (see [Esin 2014]).

The thermal cycles started with a heating at 10°C.s^{-1} and solution treatment in the austenite (+CrN) phase field at 900°C for 5 min followed by cooling at rates ranging from 40 to 60°C.s^{-1} and an isothermal treatment (IT) at 400°C for 1h (I and C samples) or 2h (N and C+N) to study the austenite decomposition. In the following, the times will be specified with respect to the time of cooling start. A unique IT temperature of 400°C was selected, in order to compare the bainite transformation at the same temperature for all the investigated steels, I, C, N and C+N (see Ms

and Bs values in Table 1). The IT durations were selected on the basis of previous dilatometry experiments.

Microstructures were observed after 4% Nital etching with scanning electron microscope (SEM) Jeol Quanta-600F. Transmission electron microscopy (TEM) thin foils were electrochemically thinned in a solution of 5% of acetic acid and 95% of perchloric acid at a temperature close to 0°C before examination in a Jeol ARM200F-FEG transmission electron microscope. Additional thin foils were prepared using Focused Ion Beam (FIB) lift out and thinning.

All thermodynamic calculations were done with the TCFE7 database and the S version of Thermocalc® software.

3 Precipitation during the enrichment treatment

In the case of N and C+N steels, the enrichment treatments were carried out in the austenite+CrN phase field. Indeed at 900°C, nitrogen content during enrichment is beyond the solubility limit in austenite (estimated to 0.1wt%) thus leading in both steels to the precipitation of CrN nitrides. Their crystallographic structure, which matches the rock salt (NaCl) structure, was identified by HEXRD as well as electron diffraction in TEM after quenching where a martensitic microstructure is formed. EDS and EELS analyses indicate a ratio N/substitutional elements close to 1. The mass fraction of the CrN nitrides, which was measured by HEXRD (Table 1), is comprised between 0.3 and 0.6wt%, depending on the samples. It does not reach the equilibrium amount, that is 1.0wt% and 1.3wt% resp. in N and C+N steels. The CrN nitrides size distribution spans a large range, from ~30 nm to 1 µm. The larger CrN nitrides tend to be more facetted. The precipitation of micro sized CrN is heterogeneous at γ grain boundaries. The smaller nitrides are intragranular and could come from temporary supersaturation in nitrogen of the austenite during the enrichment. Low density of AlN and $MnSiN_2$ nitrides was also detected by TEM. They could enhance the formation of CrN nitrides, with which they are frequently gathered. More details about these nitrides can be found in [Catteau 2016].

4 Bainite microstructure

HEXRD allowed identifying the phases present at the different stages of the thermal cycle (Figure 1a). Diffraction patterns at four chosen times are shown in Figure 1b for a C+N sample. During heating, first the tempering of martensite occurs and above Ac1 (685°C) the austenitization starts; thus, at t_1 (T=750°C, Ac_3=765°C), ferrite (α), austenite (γ), cementite (θ) and CrN phases are present. At the end of austenitizing (time t_2), only γ and CrN are present; between t_2 and t_3, cooling rate is fast enough that no phase transformation occurs; at the end of 2 h isothermal holding at 400°C (time t_4), we find α, θ, CrN and untransformed γ. All non-indicated peaks correspond to cementite orthorhombic structure, except the peak at ~3.05°, which corresponds to the Pt/Pt-Rh S thermocouple. The same phases were identified in the N sample. For the I and C samples, as expected, only α, γ and θ phases were identified.

The microstructure of a C+N sample was characterized by TEM after 85 s of isothermal holding at 400°C. Ill-defined bainitic ferrite laths, with thicknesses between 30 and 150 nm and length up to 600 nm are predominant (Figure 2a,b). Cuboidal CrN precipitates, with sizes ranging between 30 and 150 nm, are located at the interface of several ferritic domains. No clear orientation relationship between α and CrN could be established. One concludes that these CrN precipitates are probably those that were formed during the nitriding. One can see as well an example of AlN, $MnSiN_2$ and CrN nitrides aggregate. Indeed, $MnSiN_2$ precipitates (space group $Pna2_1$, Figure 2c) as well as VN nitrides were identified by TEM (electron diffraction and chemical composition analysis). Their number density remains low compared to CrN precipitates. Another C+N sample isothermally held for 2 h at 400°C was analyzed. The observations are similar to

those related to the 85 s IT, so they are not reproduced here. CrN precipitation was not detected inside the α phase.

We attribute the fine and tangled bainite microstructure to the nucleation of bainitic ferrite on the CrN nitrides, which formed during the enrichment. CrN particles could favor the ferrite nucleation through the decrease of interfacial energy [Bramfitt 1970, Ishikawa 1994], maybe also through the presence of dislocations around CrN particles [Enomoto 1998]. Chemical composition gradients around the particles (as equilibrium has not been reached during the nitriding) could also play a role [Furuhara 2003]. If no clear OR between CrN nitrides and ferrite grains could be established, it is probably because more observations are required to find one ferrite grain connected to the CrN particle that stimulated its nucleation. The small size of the ferrite grains is related the CrN nitrides number density. The hard impingement of nearby, independently nucleated ferrite grains prevented the formation of bainite sheaves, which requires autocatalytic nucleation on primary ferrite grains. The role of CrN nitrides will be substantiated as well from the analysis of phase transformation kinetics, in next Section.

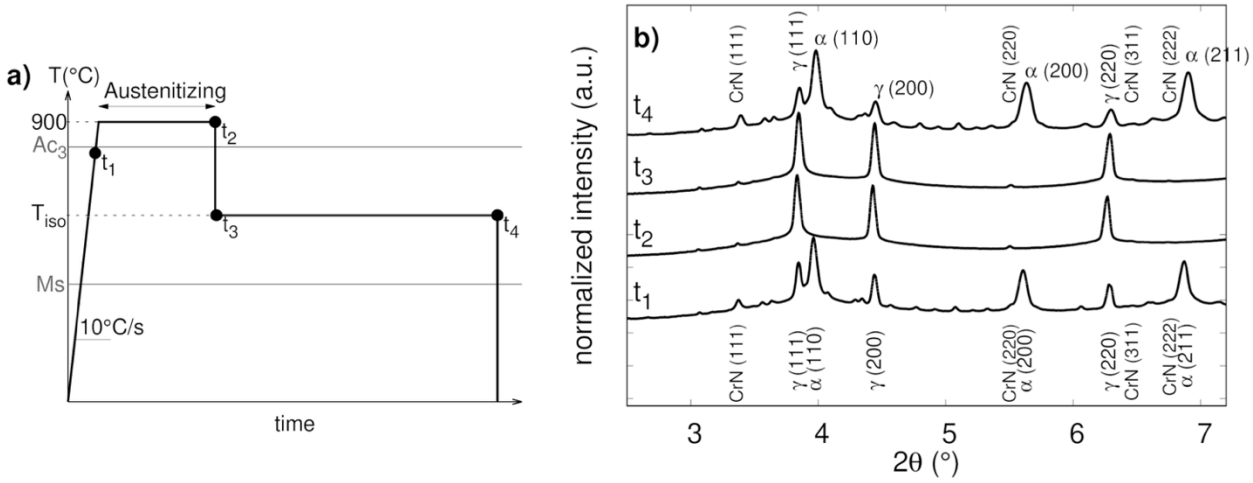

Figure 1: a) Thermal cycle; b) HEXRD patterns at different times, for a C+N sample and for an IT at 400°C. c) Example or Rietveld refinement (time t_4), in which the background has been removed.

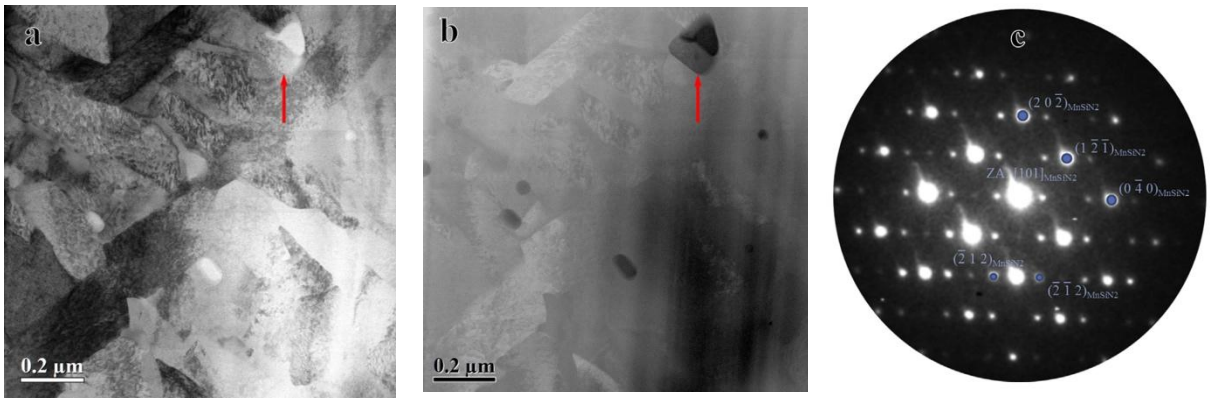

Figure 2: STEM micrographs of a C+N sample isothermally held at 400 °C for 85 s. a) bright field (BF) b) HAADF; Grains with high contrast in BF and low contrast in HAADF are bainitic ferritic grains. Particles showing a darker contrast in HAADF are nitrides. Inhomogeneity in the foil thickness causes the dark mark in the lower right corner in HAADF. The faint diagonal streaks are artefacts owed to FIB preparation. The arrow shows an AlN/$MnSiN_2$/CrN aggregate. c) Microdiffraction pattern recorded from an $MnSiN_2$ precipitate in [101] zone axis.

The phase transformation that occurs isothermally at 400°C in C+N (and probably N) samples shares some common features with intragranularly nucleated bainite, generally referred to as acicular ferrite [Bhadeshia 2001, Babu 2004, Diaz-Fuentes 2003, Gourgues 2000].

Microstructures reported in literature are much coarser than in present study: this can be related to the probably lower number density of intragranular nucleation sites (generally inclusions such as titanium oxides). Further investigations are necessary to ascertain the similarities with acicular ferrite, in particular by establishing that ferrite nucleates on CrN and by considering local orientations, as e.g. in [Gourgues 2000].

As for initial and carburized steels, coarser bainite microstructure with more usual features were obtained. These are presented in [Catteau 2016].

5 Bainite transformation kinetics

The evolutions of α, γ, θ and CrN mass fractions during holding at 400°C were obtained from the HEXRD experiments as displayed in Figure 3 (except γ, for better clarity). The I state exhibits the fastest kinetics of ferrite formation (incubation and transformation rate) due to its low carbon content. Actually, 5wt% α had already formed during cooling when the IT temperature had been reached. The cementite amount could not be quantified for this state but its orthorhombic crystal structure diffraction peaks were detected after 40 s.

In the C state, the bainitic ferrite formation kinetics was slower than in the I state, as expected considering the higher carbon amount. Ferrite formation started at 40 s. The cementite was detected at 220 s and quantified at 400 s. For both I and C states, cementite precipitation was detected once some ferrite had already been formed: 65% and 10%, respectively. Thus, according to our results, bainitic ferrite forms first in the austenite followed later by the cementite.

The enrichment in nitrogen slowed down the bainitic ferrite formation kinetics, compared to the initial steel (even if the carbon content has decreased, see Table 1). The kinetics of bainitic ferrite formation in N and C+N states were similar and intermediate between I and C states. For the same nitrogen amount in solid solution in γ (0.25wt%), in N and C+N states, higher carbon content in C+N state did not slow down significantly the kinetics. For both states, the ferrite started to form quickly: at 20 s for the N sample and during cooling for the C+N sample. The C+N state kinetics being faster than in the C state is quite surprising, as the C+N state contains a larger amount of γ-stabilizing interstitial elements. Hence, it comes out that the bainitic ferrite formation kinetics is not simply related to the total amount of carbon and nitrogen in solid solution. CrN formed in austenite during the enrichment process is thought to be responsible for the fast transformation kinetics of the C+N alloy. Indeed, CrN particles could favor the ferrite nucleation, as mentioned in previous section.

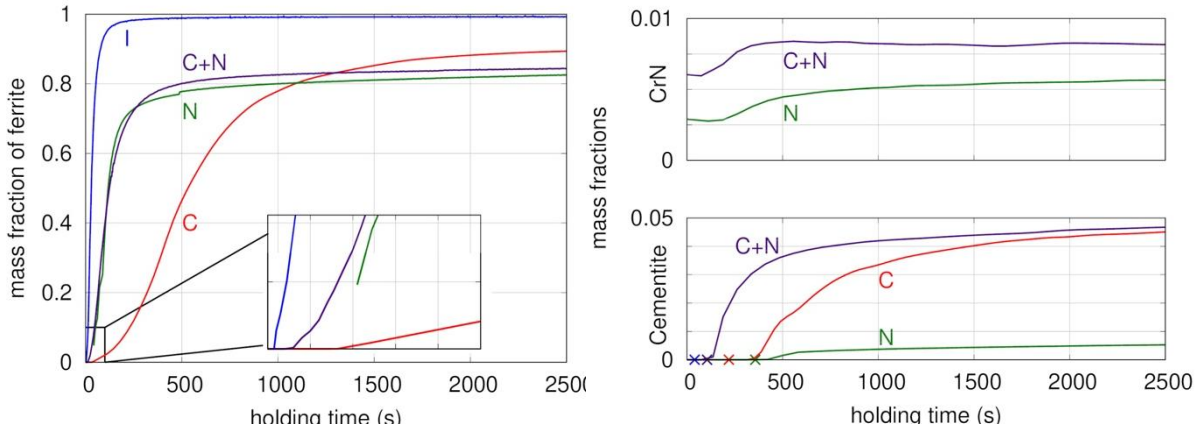

Figure 3. Evolution of the mass fraction of ferrite (with a zoom for short times), CrN and cementite during isothermal treatment at 400°C, for different interstitials concentrations, from in-situ HEXRD. The crosses show the start of cementite precipitation.

Besides, the CrN mass fraction itself increased during the IT. For both N and C+N states, this increase started after a large amount of ferrite had already formed: 71% and 55% for N and C+N states, at 190 and 160 s, respectively. This increase is due to the growth of initially present CrN nitrides, and not to the nucleation of new nitrides, in view of the absence of CrN nitrides in bainitic ferrite laths. The CrN mass fraction increase may be linked with cementite precipitation: for the N state, the cementite precipitation started after this increase, while for the C+N state, CrN and cementite formations were concomitant. Hence, possible role of CrN on cementite precipitation is highlighted.

Finally, the austenite decomposition was incomplete in all cases, except for the I state. The amount of non-transformed austenite was 0, 5, 11 and 7 wt% for the I, C, N and C+N states, respectively. This is a feature of bainite transformation, which occurs when the transformation temperature is close to Bs. In our case, the difference between Bs and the transformation temperature (400°C) is the largest for the I state (150°C) and it is smaller for the the C, N and C+N states. However, let us mention that for N and C+N states, the decomposition of austenite is not fully stabilized after 2h IT and ITs longer than 2 h would be necessary to determine the final amount of non-transformed austenite at 400°C. As for the C state, the phases amount was fully stabilized after 1h.

6 Evolutions of cell parameters

From HEXRD experiments, the evolutions of cell parameters can be analyzed too. Thus, ferrite cell parameters in I and C steels during isothermal hold at 400°C are presented in Figure 4, vs. time as well as α_b mass fraction. The asterisks indicate when cementite starts to be detected. $a_{\alpha b}$ decreases during first stages of bainite transformation, until ca. 15wt% α_b has formed. Then, $a_{\alpha b}$ remains nearly constant. The decrease (between ca. 10^{-3} Å and 3.10^{-3} Å) has the same order of magnitude as reported in previous studies [Vuorinen 2010, Hell 2012]. It is often attributed to a desaturation in carbon of ferrite laths, which would have formed with a displacive mechanism. This would explain the larger decrease in C steel than in I steel. Nevertheless, the decrease is lower than calculated assuming full desaturation [Bhadeshia 2001]. This suggests a role of internal stresses. In I steel, the decrease can also come in part from the precipitation of cementite (after 40 s). SEM observations put into evidence intra-lath cementite precipitation. However, for C steel, cementite starts to precipitate well after the decrease of $a_{\alpha b}$.

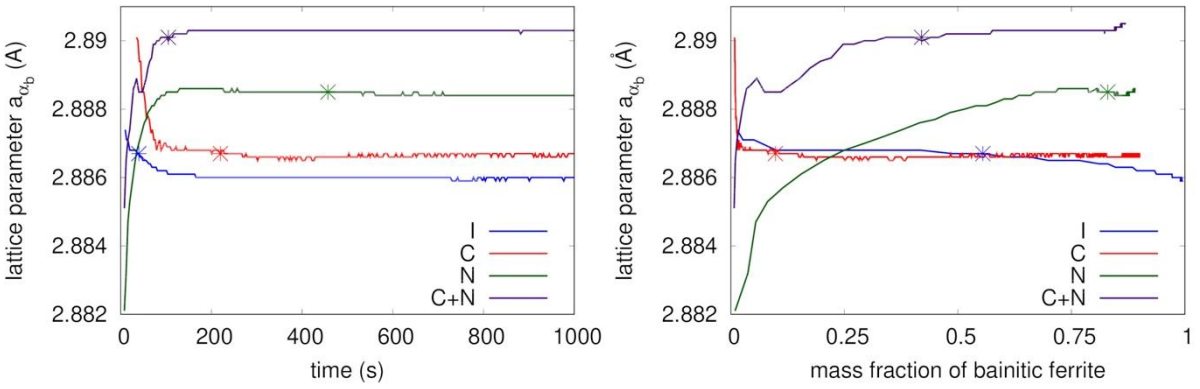

Figure 4: $a_{\alpha b}$ vs. a) time and b) α_b mass fraction, I, C, N and C+N steels. Asterisks: start of θ detection.

As for the samples containing nitrogen, $a_{\alpha b}$ increased continuously during the IT, with two stages, fast and then slow, after ca. 10wt% ferrite formation. $a_{\alpha b}$ is higher for C+N than for N steel as expected, and the magnitude of the variation is similar. We have no interpretation yet for these evolutions, except that stresses might play a predominant role.

Evolutions of a_γ in I and C steels during IT at 400°C are presented in Figure 5. a_γ increases continuously in both steels. In I steel, a_γ is nearly constant until a fraction of ca. 75% has been reached. This may lead to conclude that the austenite does not get enriched. However, cementite might precipitate inside ferrite before its detection, and despite the absence of variation of $a_{\alpha b}$. The final increase of a_γ can be associated with austenite enrichment. Nevertheless, due to the high amounts of ferrite, one cannot exclude effects of internal stresses. In C steel, the larger initial cell parameter is correlated with the higher carbon concentration in austenite, according to empirical formulae [Catteau 2017]. The increase of a_γ is lower than in I steel and a_γ seems to stabilize upon θ precipitation detection. Further increase seems to start at ca. 80% α_b formation, but longer IT duration would be necessary to confirm it.

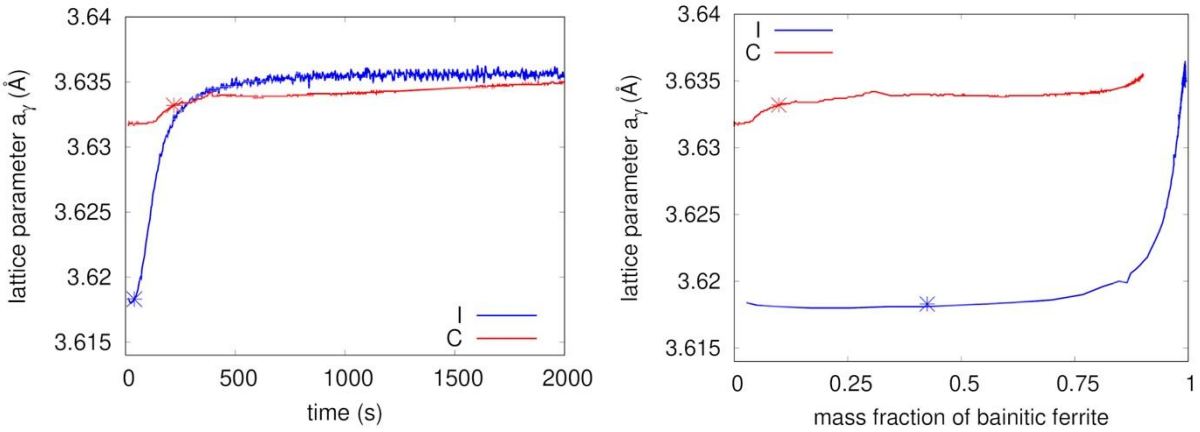

Figure 5: a_γ vs. a) time and b) α_b mass fraction, I and C steels. Asterisks: start of θ detection.

In nitrogen-enriched steels (N and C+N), an evolution of the shape of the austenite diffraction peaks was observed during the IT, as shown in Figure 6. At beginning of IT, the peaks were symmetrical, reflecting a homogeneous carbon concentration in austenite. Then, a shoulder arose at low diffraction angles. This did not occur in I and C steels, (experiments were carried out at DESY instead of ESRF). However, the FWHM was systematically higher for these experiments, which may have hidden possible asymmetry of the peaks.

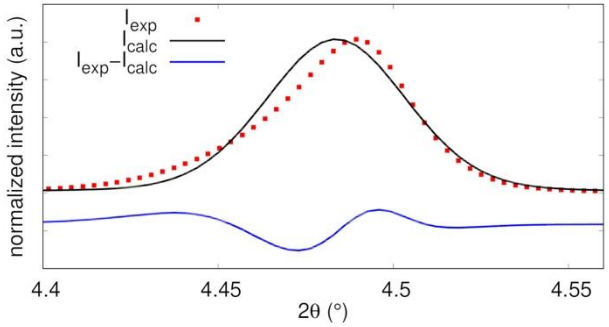

Figure 6: Example of Rietveld refinement on an asymmetric austenite {200} diffraction peak. N sample, IT 100 s.

Following previous analyses [Stone 2008, Vuorinen 2010], the austenite peaks asymmetry is attributed to heterogeneities in interstitials concentration, associated with two populations of austenite: the first one (denoted γ^{st}) with higher concentrations in carbon and nitrogen is more stable and localized between the laths of bainitic ferrite. The second one (denoted γ^{tr}) with lower concentrations corresponds to the remaining austenite undergoing the transformation. As illustrated in Figure 6, it is possible to perform a Rietveld refinement by assuming the presence of one single population of austenite, which represents sort of an average between γ^{st} and γ^{tr}. It will be termed as the global (or total, γ^T) austenite.

Following an approach introduced in [Babu 2005], the mass fractions and cell parameters associated with both populations of austenite, γ^{st} and γ^{tr}, were estimated. The results are shown in Figure 7 for a nitrided steel, together with those for the "global austenite", γ^{T}. It can be seen in Figure 7a that the increase of γ^{st} mass fraction is directly related to the one of the bainitic ferrite. This supports the assumption of a stabilization of the austenite by the rejection of carbon and nitrogen by the ferrite laths previously formed with a displacive mechanism. Similar trends were obtained with the C+N steel. In both N and C+N steels, the evolutions of a_{γ}^{tr} and a_{γ}^{T} are overlaid in first stages and then set apart due the increase of γ_{st} mass fraction (Figure 7b-c). The lattice parameter of stabilized austenite is constant and it corresponds to the final value associated with the global austenite a_{γ}^{T}.

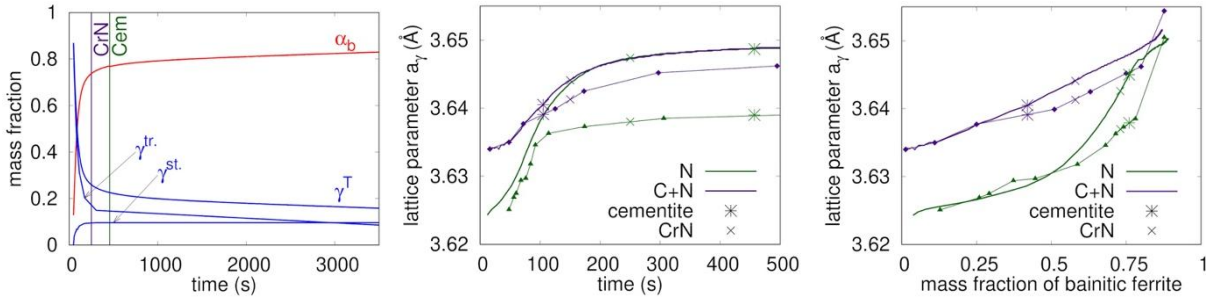

Figure 7: Evolution of: a) mass fraction of bainitic ferrite and austenite (γ^{tr}: transforming, γ^{st}: stable, γ^{T}: total or global), for N steel; b) cell parameters vs. time for N and C+N steels; c) cell parameters vs. α_b mass fraction, for γ^{T} (continuous line) and γ^{tr} (dotted line). Asterisks: start of cementite and CrN detection.

7 Elements on the bainite transformation mechanism

In situ tracking of the bainite transformation by HEXRD provides some new elements about its mechanism. Indeed, most studies based on HEXRD considered bainite structures without carbides [Hell 2011, Babu 2005, Stone 2008, Chen 2009], except in [Dutta 2014]. For I and C steels, bainitic ferrite formation precedes the precipitation of cementite, which is detected only after significant fraction of ferrite has formed. The following sequence is probable for the steels without nitrogen: formation of ferrite laths according to a displacive mechanism. The carbon in supersaturation within ferrite can either precipitate in cementite (inter- or intra-lath, depending on temperature), or enrich the untransformed austenite. If the austenite gets stabilized by the carbon, the transformation is strongly slowed down, leading to incomplete transformation. The displacive character of ferrite formation is firstly justified by the decrease of the ferrite cell parameter ($a_{\alpha b}$) at first stages of the transformation. This decrease reflects the desaturation of the ferrite laths, even if the effects of stresses do not allow to link directly $a_{\alpha b}$ to the carbon concentration in ferrite. The carbon amount in austenite when the transformation stops is also in accordance with the displacive theory. The transformation should stop when the free enthalpy of the carbon-enriched austenite is equal to the one of ferrite with the same composition. The "T_0 curve" shows this concentration as a function of temperature. The T'_0 curve takes into account the elastic energy stored in ferrite, which increases its Gibbs energy. These curves are plotted in Figure 8 and compared to experimental points, which are deduced from the cell parameter of austenite, with the following empirical rule [Catteau 2017]:

$$a^{\gamma}(T)=[3.63067+0.049wt\%(C+N)^{\gamma}].\left[1+\left(24.92\ 10^{-6}-2.51\ 10^{-6}wt\%(C+N)^{\gamma}\right).(T-1000)\right] \qquad (1)$$

where a^{γ} is in Å, $wt\%(C+N)^{\gamma}$ is the mass concentration in carbon and nitrogen in solid solution in austenite and T the temperature in K. This formula is in accordance with various references compiled in [Scott 2007]. The parameters were adjusted on the basis of our experiments. It can be seen in Figure 8 that the experimental points are well aligned on the T'_0 curve assuming an elastic energy of 600 $kJ.mol^{-1}$, which is realistic in view of the literature.

As for nitrogen-enriched steels (N and C+N), it is more difficult to propose a transformation mechanism regarding the diffusive or displacive character of the bainite transformation. The cell parameter $a_{\alpha b}$ increases continuously during the IT, which suggests an important influence of the stresses. For both steels, the T_0 analysis (Figure 8b) does not seem to work as well as for I and C steels. The T_0 curve was calculated by assuming a zero concentration of nitrogen in ferrite and austenite. Indeed, we assumed that all the nitrogen is consumed by the formation of the CrN nitrides during the bainite transformation. The same assumption was done to calculate the composition of the austenite with equation (1) from the lattice parameters determined from HEXRD. The agreement with the experiment is good, but the absence of accounting of stored elastic strain energy in ferrite represents a large discrepancy with respect to the steels without nitrogen. The analysis of austenite cell parameter puts into evidence the rejection of interstitials from bainitic ferrite to austenite, leading to composition heterogeneities in this phase. Besides, for both steels, the sequence of ferrite preceding carbides and nitrides precipitation is preserved. Concomitant precipitation of both phases suggests some interactions, but there are no microstructural observations to confirm this.

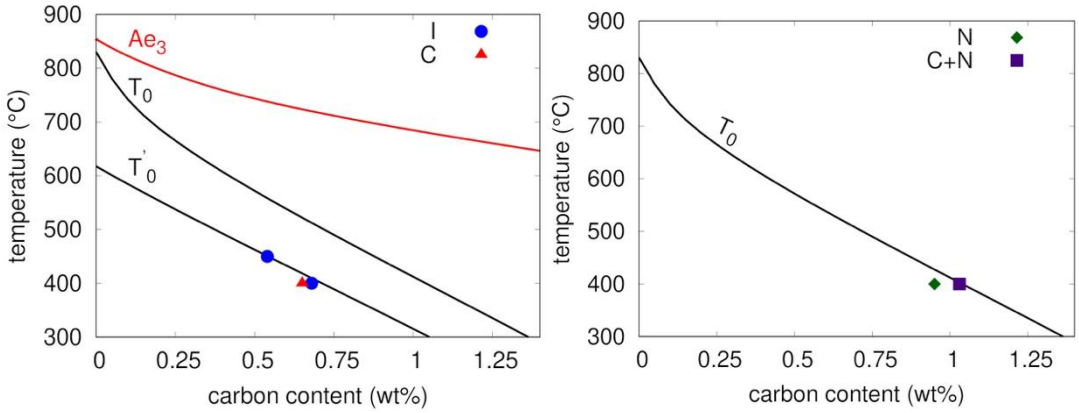

Figure 8: Comparison between carbon concentrations within austenite at the end of bainite transformation with T_0 and T'_0 concepts, considering an elastic strain energy of 600 J.mol^{-1} stored in ferrite. a) I and C steels; b) N and C+N steels.

8 Conclusion

Effects of carbon and nitrogen on bainite transformation have been studied in a low alloyed steel, by HEXRD and TEM. Experimental study of isothermal transformation kinetics was realized on specimens homogeneously enriched (in carbon and/or nitrogen) in the austenitic field. Classical slowing down effect on kinetics was observed by increasing the carbon content in parent austenite. In presence of nitrogen, kinetics cannot be directly linked to the interstitials content in austenite. Kinetics is intermediate between initial and carbon enriched steels and a finer microstructure is observed. This phenomenon is attributed to the stimulation of ferrite nucleation by the presence of CrN in parent austenite, which precipitated during enrichment. In presence of nitrogen, the bainite microstructure consists of submicronic, ill-defined and tangled laths, which is attributed as well to the nucleation on CrN nitrides. In situ HEXRD allowed to analyse the evolutions of the different phases: ferrite, austenite, cementite and CrN. To our knowledge, similar studies were carried out almost only on carbide-free bainite and steels without nitrogen. The chronology of the phases formation could be established, as well as the evolutions of the cell parameters. For initial and carburized steels, the results are in agreement with the assumption of a displacive mechanism. In presence of nitrogen, analysis of austenite cell parameters and peaks profiles showed clearly the rejection of interstitials from ferrite into austenite, leading to composition heterogeneities, without making possible to propose firm hypotheses on the phase transformation mechanism.

Acknowledgement

This work was supported by PSA and by the French State through the program "Investment in the future" operated by the National Research Agency (ANR) and referenced by ANR-11-LABX- 0008-01 (LabEx DAMAS).

References

Babu S.S.: The mechanism of acicular ferrite in weld deposits, Curr. Opin. Solid State Mater. Sci., Vol 8, 2004, p. 267-278.

Babu S.S, Specht E.D., David S.A., Karapetrova E., Zschack P., Peet M, Bhadeshia H.K.D.H.: In-situ observations of lattice parameter fluctuations in Austenite and transformation to Bainite, Met. Mat. Trans. A, Vol 36A, No 12, 2005, p. 3281-3289.

Bhadeshia H.K.D.H., David S.A., Vitek J.M., Reed R.W.: Stress Induced Transformation to Bainite in Pressure Vessel Steel. Materials Science and Technology, Vol 7, 1991, p. 686–698.

Bhadeshia H.K.D.H.: Bainite in Steels: Transformations, Microstructure and Properties, second ed., IOM Communications Ltd, 2001.

Böttger A., van Genderen M. J., Sijbrandij S.J., Mittemeijer E.J., Smith D.W.: Atom probe and X-ray diffraction analysis of the composition and structure of precipitates formed on tempering of ternary iron-carbon-nitrogen martensites, ISIJ Int., Vol 36, No 7, 1996, p. 764-767.

Bramfitt B.: The effect of carbide and nitride additions on the heterogeneous nucleation of liquid iron, Metall. Trans., Vol 1, 1970, p. 1987-1995.

Catteau S.D, Denis S., Teixeira J., Dulcy J., Dehmas M., Redjaïmia A., Courteaux M.: Munich, Germany, in: H.-W. Zoch, R. Schneider, T. Lübben (Eds.), Proc. 21st IFHTSE Congress, AWT, Bremen, Germany, 2014, pp. 153-161.

Catteau S.D, Van Landeghem H.P., Teixeira J., Dulcy J., Dehmas M., Denis S., Redjaïmia A., Courteaux M.: Carbon and nitrogen effects on microstructure and kinetics associated with bainitic transformation in a low-alloyed steel, J. Alloys and Compounds, Vol 658, 2016, p. 832-838.

Catteau S.D. : Effets du carbone et de l'azote sur les cinétiques de décomposition de l'austénite dans un acier faiblement allié – Etude expérimentale et Modélisation, PhD. Thesis manuscript, 2017, (in preparation).

Chen X., Vuorinen E.: In-situ high temperature X-ray studies of austempering transformation in high silicon cast steel, ISIJ Int., Vol 49, No 8, 2009, p. 1220-1224.

Constant A., Henry G., Charbonnier J-C., Principes de Base des Traitements Thermiques, Thermomecaniques et Thermochimiques des Aciers, PYC Edition, 1992.

Cheng L., Böttger A., Mittemeijer E.J.: Tempering of iron-carbon-nitrogen martensites: Metall. Mat. Trans. A, Vol 23A, 1992, p. 1129-1145.

Diaz-Fuentes M., Iza-Mendia A., Gutierrez I.: Analysis of different acicular ferrite microstructures in low-carbon steels by electron backscattered diffraction. Study of their toughness behavior, Metall. Trans. A, Vol 34A, 2003, p. 2505-2516.

Dutta R.K., Huizenga R.M., Amirthlingam M., King A., Gao H., Hermans M.J.M., Sietsma J., Richardson I.M: In-situ synchrotron diffraction studies on transformation strain development in a high strength quenched and tempered structural steel. - Part I. Bainitic transformation, Metall. Mat. Trans. A, Vol 45A, 2014, p. 218-229.

Enomoto M.: Nucleation of phase transformations at intragranular inclusions in steel, Metals Mater. Korea, Vol 4, No 2, 1998, p. 115-123.

Esin V.A., Denand B., Le Bihan Q., Dehmas M., Teixeira J., Geandier G., Denis S., Sourmail T., Aeby-Gautier E.: In situ synchrotron X-ray diffraction and dilatometric study of austenite formation in a multi-component steel: Influence of initial microstructure and heating rate, Acta Mat., Vol 80, 2014, p. 118-131.

Furuhara T., Yamaguchi J., Sugita N., Miyamoto G., Maki T.: Nucleation of proeutectoid ferrite on complex precipitates in austenite, ISIJ Int., Vol 43, No 10, 2003, p. 1630-1639.

Gourgues A-F., Flower H.M., Lindley T.C.: Electron backscattering diffraction study of acicular ferrite, bainite, and martensite steel microstructures, Mater. Sci. Technol., Vol 16, 2000, p. 26-40.

Hell J-C., Dehmas M., Allain S., Prado JM., Hazotte A., Chateau J-P.: Microstructure-properties relationships in carbide-free bainitic steels, ISIJ Int., Vol 51, No 10, 2011, p. 1724-1732.

Hell J-C.: Aciers Bainitiques Sans Carbure : Caractérisations Microstructurale Multi-Echelle et In-Situ de la Transformation Austénite-Bainite et Relations entre Microstructure et Comportement Mécanique. PhD. Thesis manuscript, Université Paul Verlaine - Metz, 2012.

Ishikawa F., Takahashi T., Ochi T., Intragranular ferrite nucleation in medium-carbon vanadium steels, Metall. Mat. Trans. A, Vol 25, No 5, 1994, p. 929-936.

Jiang Z., Li X., Gu J., Hu M., Zhu Z.: Isothermal decomposition behavior of the high nitrogen concentration γ-Fe[N] prepared from pure iron, Appl. Surf. Sci., Vol 254, 2008, p. 7361-7364.

Nakada N., Fukuzawa N., Tsuchiyama T., Takaki S., Koyano T., Iwamoto T., Omori Y.: Isothermal transformation in Fe-N hypereutectoid alloy, ISIJ Int., Vol 53, No 1, 2013, p. 139-144.

Scott C. P., Drillet J.: A study of the carbon distribution in retained austenite, Scripta Mat., Vol 56, 2007, 489-492.

Simon A., Lorenzo A., Beck G., Meynet G. : Influence de la teneur en azote sur les transformations de l'austénite carbonitrurée de l'acier 30CD4, Mémoires Sci. Rev. Mét., Vol 71, No 12, 1974, p. 823-831.

Stone H.J, Peet M.J., Bhadeshia H.K.D.H., Withers P.J., Babu S.S., Specht E.D.: Synchrotron X-ray studies of austenite and bainitic ferrite, Proc. R. Soc. A, Vol 464, 2008, 1009-1027.

Vuorinen E., Chen X.: In Situ High Temperature X-Ray Studies on Bainitic Transformation of Austempered Silicon Alloyed Steels, Materials Science Forum, Vol 638-642, 2010, p. 3086–3092.